Journal of the Geological Society, London, Vol. **149**, 1992, pp. 193–207, 11 figs, 6 tables. Printed in Northern Ireland

DUPL

Petrology and dynamics of the Waimihia mixed magma eruption, Taupo Volcano, New Zealand

S. BLAKE,[1] C. J. N. WILSON,[2] I. E. M. SMITH,[3] & G. P. L. WALKER[4]

[1]*Department of Earth Sciences, The Open University, Walton Hall, Milton Keynes, MK7 6AA*

[2]*Department of Earth Sciences, University of Cambridge, Downing Street, Cambridge CB2 3EQ*

[3]*Department of Geology, University of Auckland, Private Bag, Auckland, New Zealand*

[4]*Hawaii Institute of Geophysics, 2525 Correa Road, Honolulu, Hawaii 96822, U.S.A.*

Abstract: The Waimihia pumice deposit was erupted from Taupo volcano about 3.3 ka BP. It comprises a plinian tephra fall deposit divisible into two volumetrically subequal fall units and a late-stage, volumetrically minor, near-vent ignimbrite. About 7.5 km^3 of magma were erupted at an average rate of *c.* 8×10^8 kg s^{-1}. Whole rock, glass and mineral compositions define three crystal-poor magma types: rhyolite, rhyodacite and andesite. The proportions of the three magmas varies with stratigraphic position in the two fall units. The lower Waimihia fall unit shows a steady upward increase in rhyodacite from $<1\%$ to 5.5% and a near absence of andesite ($<0.05\%$). Rhyodacite in the upper Waimihia fall unit decreases upward from 28% to 2% while andesite increases (0.2% to 0.8%) before decreasing (0.3%). The composition of the ignimbrite coincides with that of the top part of the upper fall unit (consistent with its stratigraphic position), suggesting that partial column collapse occurred towards the close of activity. Rhyolite dominates the total Waimihia deposit (*c.* 92%) and is similar to other post-22 ka Taupo rhyolites in terms of major element, trace element and Sr isotope composition, mineralogy and Fe-Ti oxide temperature and oxygen fugacity. The rhyodacite (*c.* 7.3%) formed by hybridization of rhyolite and andesite prior to the eruption, and occurs as grey pumices and with rhyolite in streaky pumices. Andesite (*c.* 0.3%) occurs as black scoria, sometimes containing traces of rhyodacite; it is an unusual high TiO_2 tholeiitic andesite whose $^{87}Sr/^{86}Sr$ ratio of 0.7062 is indistinguishable from that of the rhyolite. The heterogeneous pumice and scoria clasts were formed in a second magma mixing process that was active when the magmas were being transported to the surface during the eruption. The order in which the magmas were erupted, and the decoupling of the peaks in rhyodacite and andesite production, are explained by withdrawal from a three-layer sill that had formed following the injection of *c.* 0.16 km^3 of andesite into a $\geq$ 7.5 km^3 sill-shaped rhyolitic magma chamber.

Taupo volcano is one of two potentially active rhyolitic caldera volcanoes in the central segment of the Taupo Volcanic Zone, one of the world's most productive areas of silicic volcanism (Wilson *et al.* 1984, 1986; Fig. 1). Taupo has been active for over 50 000 years and at least twenty explosive and/or effusive eruptions have occurred in the past *c.* 10 000 years (Vucetich & Pullar 1973 C. J. N. W. Unpublished data). Eight of these eruptions produced ejecta volumes $\geq$0.5 km^3, the latest and largest event being the 1800 year BP Taupo eruption (Wilson & Walker 1985). All but one of these eight eruptions involved magmas with remarkably homogeneous compositions (Ewart 1963; Froggatt 1982; Dunbar *et al.* 1989*a*), in contrast to many eruptions of comparable volume from other silicic centres (e.g. Hildreth 1981). The exception is the Waimihia eruption, which took place at 3300 ^{14}C years BP (Froggatt & Lowe 1990) generating a voluminous plinian fall deposit (Walker 1981) and, during its closing stages, modest volumes of non-welded ignimbrite. Although these deposits are dominantly rhyolitic, Ewart (1963) in a regional study of Taupo Volcanic Zone rhyolites noted the presence of streaky and homogeneous grey pumices in the Waimihia deposits, whilst Walker (1981) also reported juvenile mafic clasts. This is one of the few cases in the Taupo Volcanic Zone where co-existing liquids of clearly contrasting composition were erupted. Because of this unusual feature we have carried out an integrated volcanological and petrological study of the Waimihia deposits in order to investigate the role of the rarely-erupted mafic magma in controlling the dynamics of the Taupo rhyolitic system.

Physical volcanology

The Waimihia fall deposit was studied in detail by Walker (1981) and can be divided into two fall units (named the lower and upper Waimihia) which have different dispersal axes (Fig. 1) but similar volumes and grain-size characteristics. Walker postulated that the vent was positioned at Horomatangi Reefs in Lake Taupo on the basis of maximum-clast-size data and the intersection of the two dispersal axes. The top of the lower Waimihia is identified by a slightly finer band, while the top part of the proximal upper Waimihia is somewhat finer grained and contains some poorly sorted fine-ash-rich beds in areas up to several tens of kilometres from source. Apart from these aspects the two portions are of very uniform and similar grain-size, indicative of equally powerful phases of sustained plinian activity.

The volumes of the fall deposits cannot be determined accurately because large amounts of material were dispersed over the Pacific Ocean. Two methods can be used to estimate the total volume of tephra. The first relies on integrating extrapolated exponentially decaying trends of thickness versus square root of area over infinite area (Pyle 1989). This yields bulk-volume estimates of 8.2 and 7.9 km^3 respectively for the lower and upper Waimihia (Fig. 2a), approximately equivalent to 2.0 and 1.9 km^3 of non-vesicular magma and 0.16 and 0.15 km^3 of lithic debris. The second method (Walker 1980, 1981) measures the mass of loose crystals in the fall deposit and relates this to an equivalent mass of vitric material using

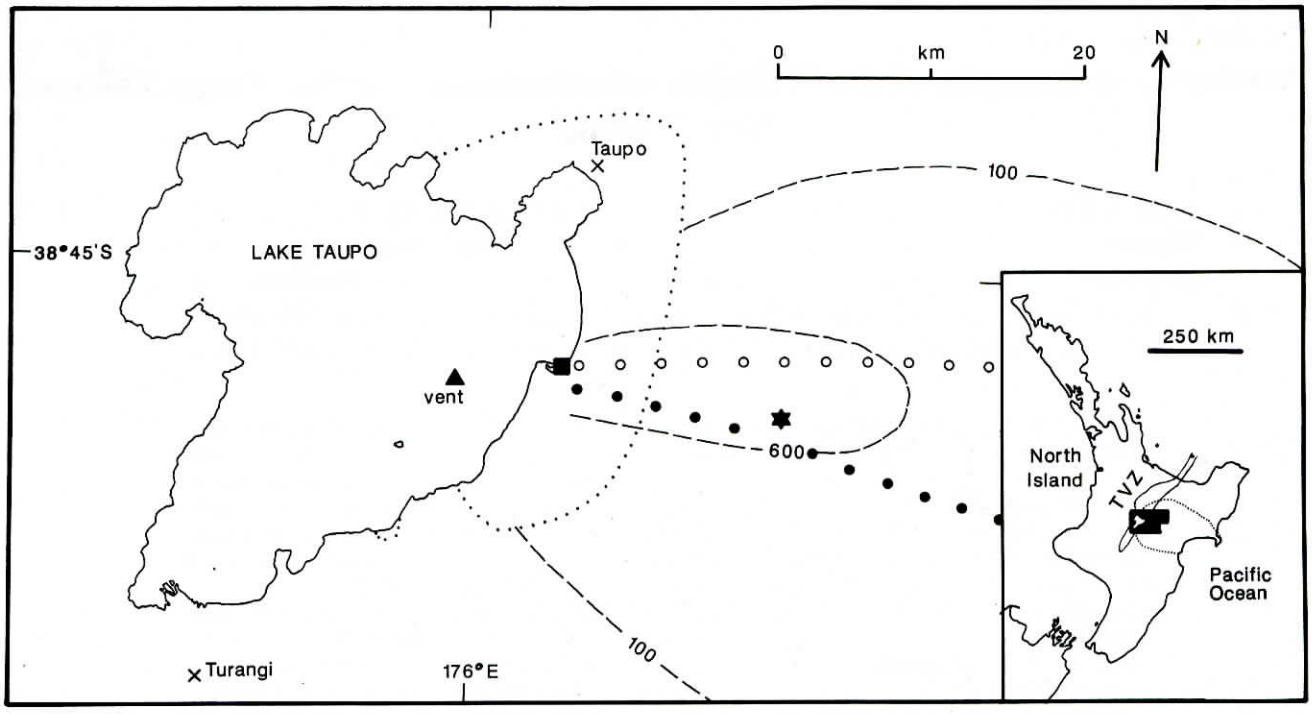

Fig. 1. Map of the Lake Taupo area, showing (after Walker 1981) vent position for the Waimihia eruption (filled triangle), 100 and 600 cm isopachs for the Waimihia fall deposit, dispersal axes for the lower (open circles) and upper (filled circles) Waimihia fall units (see text), outer limit of the Waimihia ignimbrite (dotted line), and positions of measured section (star: grid reference U18/901580, 1:50 000 sheet, New Zealand metric map grid) and ignimbrite sampling locality (square: U18/764618). Inset shows the position of the study area in the North Island of New Zealand, the 12 cm isopach (dotted line), and the outline of the Taupo Volcanic Zone (continuous line).

the crystal:vitric ratio measured in large pumice clasts. This vitric material, all <2 mm in size, has largely been dispersed over the Pacific and hence cannot be measured by direct techniques. The total mass of fall material derived by this technique is strongly dependent on the crystal:vitric ratio inferred for the original magma. Assuming a crystal:vitric ratio of 3.3:96.7 (Walker 1981) yields a total mass of *c.* 1.8×10^{13} kg, equivalent to 7.2 km^3 of magma and 0.6 km^3 of lithic debris. We consider the masses and volumes obtained by these two methods to represent likely extremes of eruption size.

In addition, non-welded ignimbrite occurs above the fall deposits within a maximum distance of 20 km from vent (Healy *et al.* 1964; Walker 1981), but its volume is difficult to assess because of burial by younger eruptives and concealment beneath Lake Taupo. Onshore deposits have a bulk volume of *c.* 0.4 km^3; doubling this to allow for material beneath Lake Taupo, and using an average measured density of 1100 kg m^{-3} and lithic content of 17% (C.J.N.W. unpub. data), makes the ignimbrite volume equivalent to *c.* 0.3 km^3 of magma and *c.* 0.06 km^3 of lithic debris. The maximum total eruption volume is thus inferred to be *c.* 7.5 km^3 of magma and *c.* 0.65 km^3 of lithic debris.

New data on the dispersal of the maximum pumice and lithic clast sizes show exponential decay of ln (size) with square root of area (cf. Pyle 1989; Fig. 2b, c). These data illustrate the close similarity of the dispersal characteristics of the lower and upper fall deposits. The dispersal of pyroclasts of a given size and density increase with the eruptive discharge rate (and thus column height). Carey & Sparks (1986) and Wilson & Walker (1987) have presented models of plinian eruption columns that allow the maximum discharge rate to be estimated from the cross-wind dispersal of the largest pyroclasts. Carey & Sparks's model indicates peak column heights of 48 and 45 km for the lower and upper Waimihia (i.e. essentially identical within errors); these translate into mass discharge rates of 9.4×10^8 kg s^{-1} and 7.3×10^8 kg s^{-1}. Wilson & Walker's model is in broad agreement, indicating discharge rates of somewhat less than 10^9 kg s^{-1}. Both Waimihia eruptions rank among the highest discharge plinian events (cf. Carey & Sigurdsson 1989).

Lithological variations in the Waimihia juvenile clasts correlate with eruption stratigraphy (Fig. 3). The lower Waimihia consists almost entirely of white rhyolitic pumice together with minor amounts of pale grey/white streaky pumice. The upper Waimihia and the ignimbrite contain variable quantities of white, grey and streaky pumice, and black dense to scoriaceous juvenile ejecta. In order to document changes in magma proportions during the eruption, a thick section of the fall deposit was logged and sampled and a single site sampled in the ignimbrite (Figs 1 and 3). In all samples, the $\geqslant 2$ mm juvenile clasts were divided into seven categories, viz: (1) pure white; (2) streaky, $<5\%$ grey; (3) banded, 5–50% grey; (4) banded, 50–95% grey; (5) banded, $>95\%$ grey; (6) pure grey; and (7) black, and their relative proportions by mass recorded. From analytical data, given below, it was established that the colour variations reflected three chemically distinctive end-members (i.e. white = rhyolite, grey = rhyodacite, black = andesite), and so the various proportions of different homogeneous and streaky clasts could be reduced to proportions of rhyolite, rhyodacite and andesite magmas.

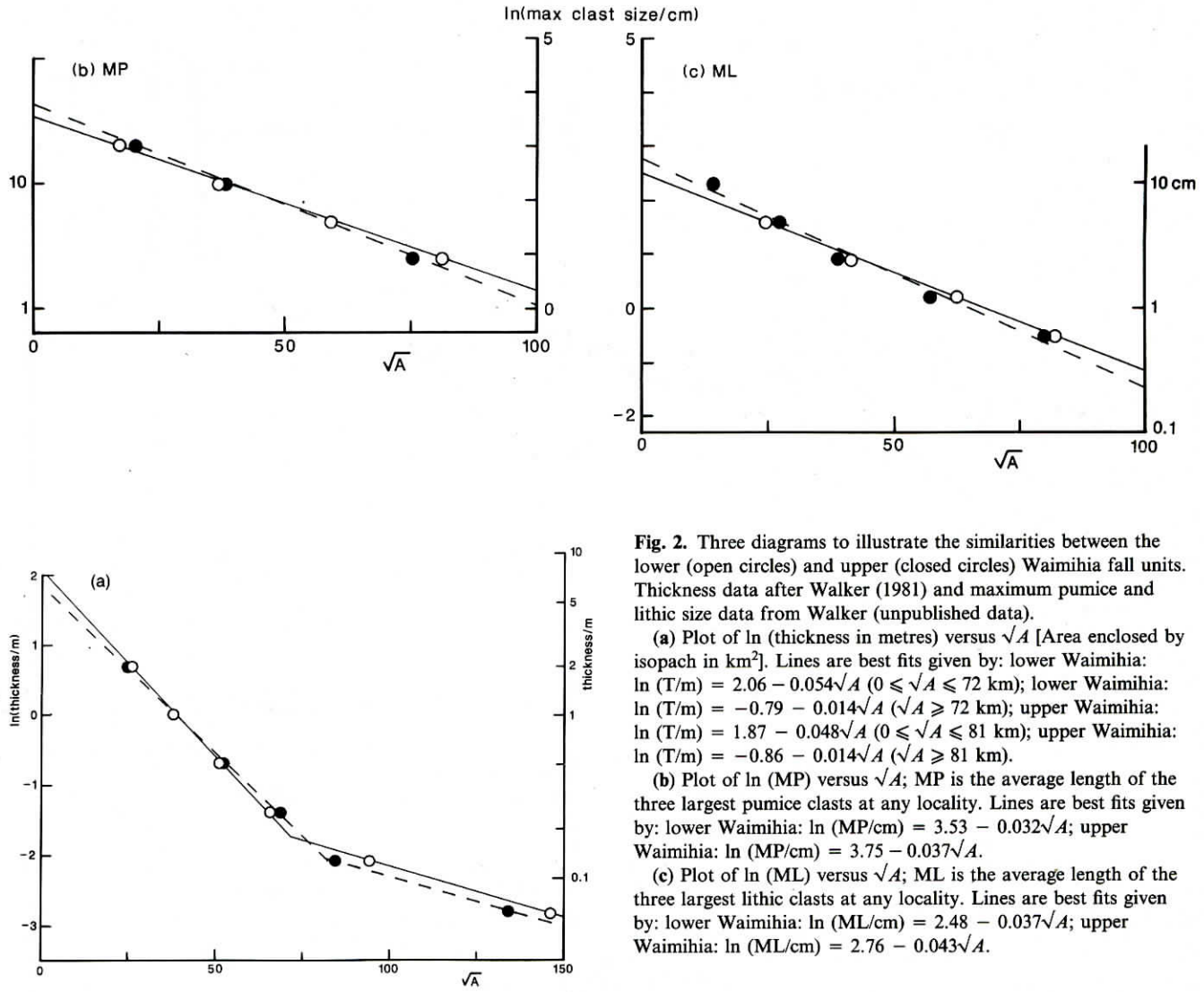

Fig. 2. Three diagrams to illustrate the similarities between the lower (open circles) and upper (closed circles) Waimihia fall units. Thickness data after Walker (1981) and maximum pumice and lithic size data from Walker (unpublished data).

(**a**) Plot of ln (thickness in metres) versus $\sqrt{A}$ [Area enclosed by isopach in km^2]. Lines are best fits given by: lower Waimihia: $\ln (T/m) = 2.06 - 0.054\sqrt{A}$ ($0 \leqslant \sqrt{A} \leqslant 72$ km); lower Waimihia: $\ln (T/m) = -0.79 - 0.014\sqrt{A}$ ($\sqrt{A} \geqslant 72$ km); upper Waimihia: $\ln (T/m) = 1.87 - 0.048\sqrt{A}$ ($0 \leqslant \sqrt{A} \leqslant 81$ km); upper Waimihia: $\ln (T/m) = -0.86 - 0.014\sqrt{A}$ ($\sqrt{A} \geqslant 81$ km).

(**b**) Plot of ln (MP) versus $\sqrt{A}$; MP is the average length of the three largest pumice clasts at any locality. Lines are best fits given by: lower Waimihia: $\ln (MP/cm) = 3.53 - 0.032\sqrt{A}$; upper Waimihia: $\ln (MP/cm) = 3.75 - 0.037\sqrt{A}$.

(**c**) Plot of ln (ML) versus $\sqrt{A}$; ML is the average length of the three largest lithic clasts at any locality. Lines are best fits given by: lower Waimihia: $\ln (ML/cm) = 2.48 - 0.037\sqrt{A}$; upper Waimihia: $\ln (ML/cm) = 2.76 - 0.043\sqrt{A}$.

Grain-size variations and maximum-clast-size data on the lower and upper Waimihia units show that discharge rates remained relatively uniform throughout the eruption, except for the finer top to the upper Waimihia. However, this finer top has juvenile clast proportions which closely match those seen in the Waimihia ignimbrite. This and the stratigraphic position of the ignimbrite are consistent with generation of the ignimbrite in the closing stages of the eruption by partial column collapse, or choking of the vent by ejecta (cf. Taupo early flow units, Wilson & Walker 1985). If the discharge rate is thus taken as being uniform, then the clast proportions can be used to measure, to a first approximation, the changing proportions of the three magma types with time. Furthermore, if the relative magma volumes in the lower and upper Waimihia are taken to be proportional to their relative bulk volumes as indicated by exponential decay data (Fig. 2a), then the total erupted volumes of the three magma types in the fall deposits and ignimbrite can be estimated. This approach gives maximum (Walker's method) volumes of *c.* 7.0 km^3 rhyolite, *c.* 0.55 km^3 rhyodacite and *c.* 0.02 km^3 andesite. The rhyodacite is a 3:1 mixture of rhyolite and andesite, so that the original magmas involved consisted of *c.* 7.4 km^3 rhyolite and *c.* 0.16 km^3 andesite.

Single clast chemical compositions

Three magma types, rhyolite, rhyodacite and andesite are recognized in the juvenile Waimihia ejecta on the basis of chemical composition, mineralogy and mineral compositions. These magma types are represented in the deposits thus (Fig. 3):

pure white pumices: rhyolite	(*c.* 75% SiO_2)
streaky pumices: mixtures of white rhyolite and grey rhyodacite	(71–75% SiO_2)
pure grey pumices: rhyodacite	(*c.* 71% SiO_2)
black scoria: andesite	(*c.* 59% SiO_2)

The black scoria contain only minor amounts of visible rhyolite and rhyodacite contamination, and do not form a separate component in the mixed, streaky pumices.

Thirteen analyses of white rhyolitic pumices collected from throughout the Waimihia deposit plot as a tight cluster in chemical variation diagrams (Fig. 4). The compositional variation between individual clasts is comparable with analytical errors, while the mean composition (Table 1) is nearly identical to that given by Ewart (1963) for Waimihia glass.

Streaky pumices have compositions which define linear arrays on variation diagrams (Fig. 4) that extend from rhyolite

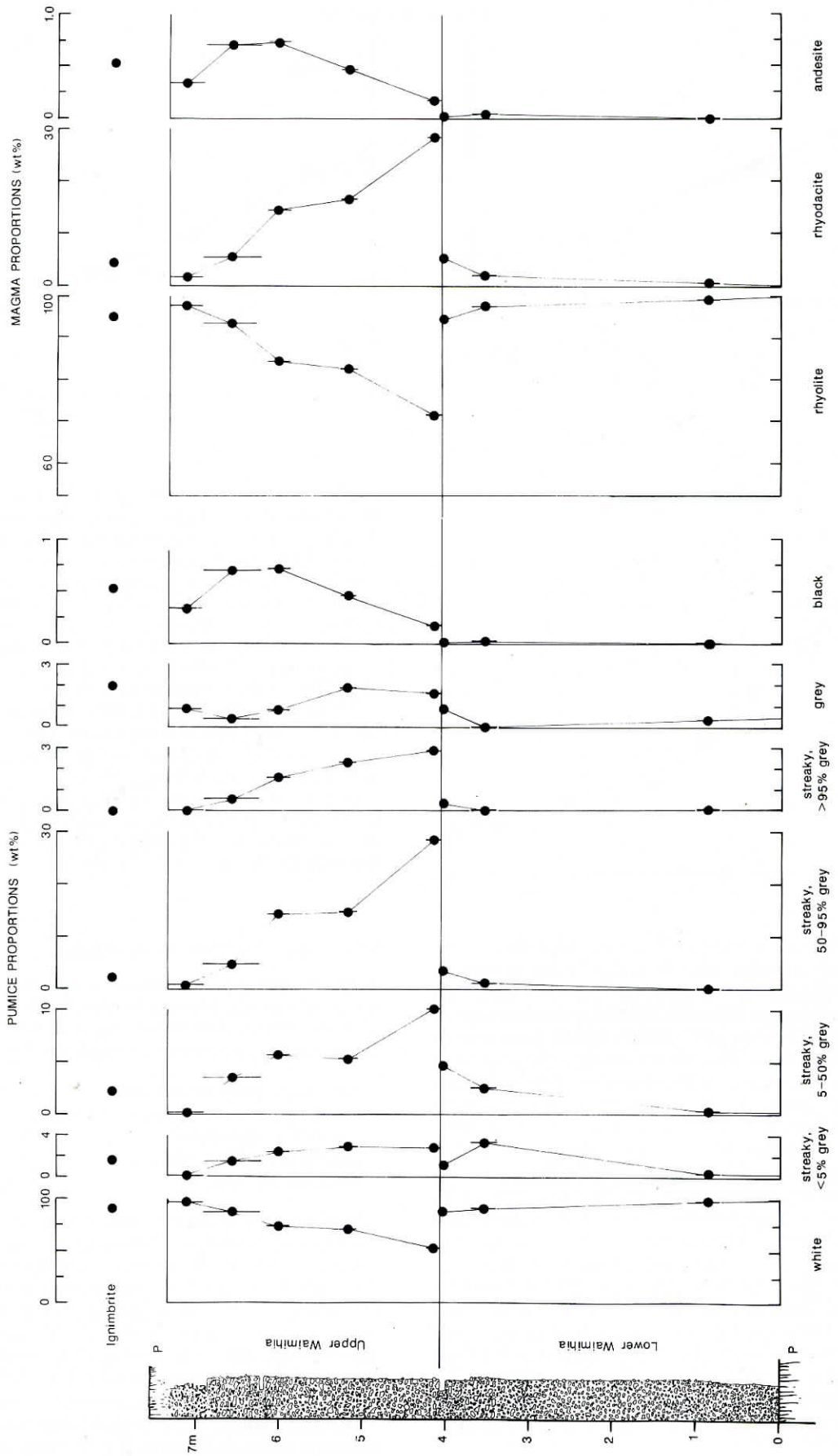

Fig. 3. Proportions of pumice types (measured in ⩾2 mm material and recalculated to 100%) and corresponding magma proportions through the measured section in the Waimihia fall deposit (Fig. 1), and from an ignimbrite sample.

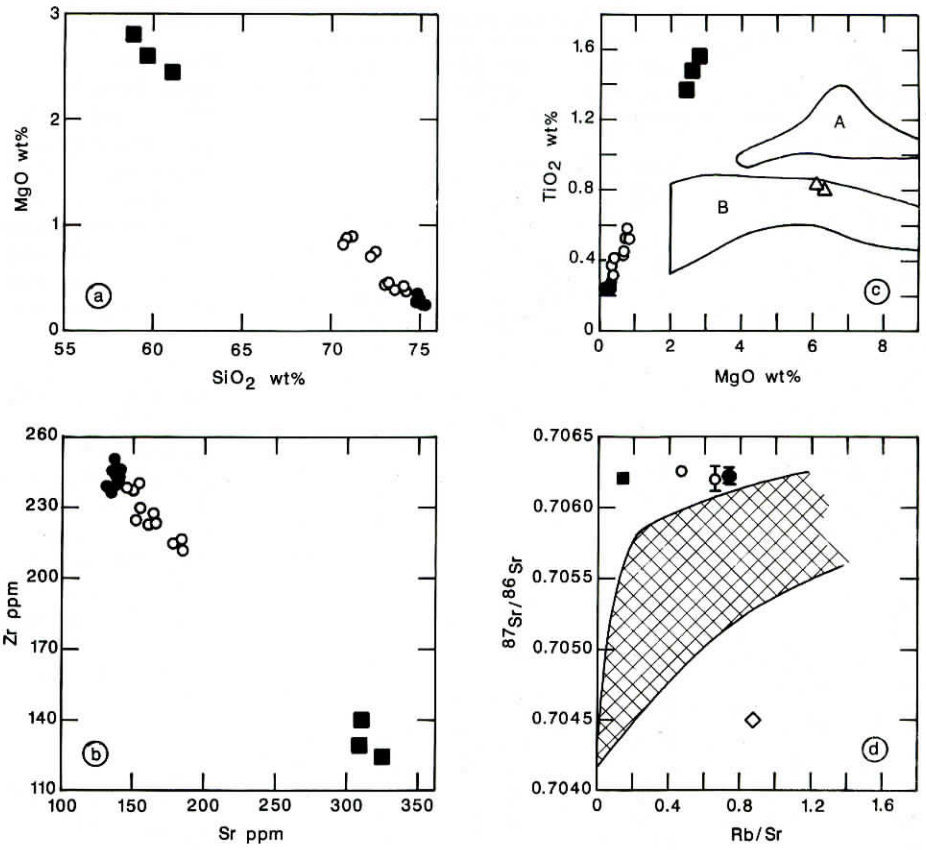

Fig. 4. Variation diagrams of single-clast analyses. Filled circles, white pumices; open circles, streaky and grey pumices; filled squares, scoria.
(**a**) MgO versus SiO_2, (**b**) Zr versus Sr; (**c**) TiO_2 versus MgO; High alumina basalts from silicic Taupo Volcanic Zone centres occupy field A except for the Tarawera 1886 and Rotokawau basalts (triangles). Field B encloses analyses with >2% MgO from stratovolcanoes. (Data from Cole 1979; Wilson & Smith 1985; Graham & Hackett 1987; Gamble *et al.* 1990.) (**d**) $^{87}Sr/^{86}Sr$ versus Rb/Sr. Diamond and shaded field defined by data from other Taupo Volcanic Zone volcanics (excluding welded ignimbrite samples) from Cole (1979), Graham & Hackett (1987) and Graham & Worthington (1988).

(*c.* 75% SiO_2) to rhyodacite (*c.* 71% SiO_2), the latter represented by a homogeneous grey pumice clast (P476/1, Table 1). As might be expected, the greater the proportion of white material, the closer the streaky pumice clast composition approaches that of the rhyolite end member, consistent with incomplete mixing between rhyodacite and rhyolite magmas.

Analyses of three black andesitic scoria fragments plot as a linear extrapolation of the rhyolite/rhyodacite data (Fig. 4), but are separated from the rhyodacite by a silica gap of 10%. On all variation diagrams a line connecting the composition of the most mafic scoria with that of the average rhyolite adequately describes all the other analyses and our interpretation is that andesite-rhyolite mixing is ultimately responsible for the compositional variability in the Waimihia samples. The rhyodacite of Table 1 is a blend of 75% rhyolite and 25% andesite.

Some scoria clasts represent an andesitic magma which has been contaminated to varying degrees with more silicic magma. This is superficially seen in a subtle mottling of many scoria clasts, while adhering patches of white, vesicular material are occasionally found. In thin section these textures are manifest in a network of pale veins dividing the rock into a sub-mm to sub-cm patchwork. Larger areas of highly vesicular silicic blebs also occur. However, scoria clast P79A (Table 1) appears free of contamination and is thought to most closely represent the end-member andesite composition. This composition is that of an acid medium-K tholeiitic andesite (nomenclature of Gill 1981), which is clearly different from other andesites in the Taupo Volcanic Zone (cf. Cole 1979). The latter are calc-alkaline andesites with FeO_t/MgO ratios of 1 to 2 and TiO_2 contents of less than 0.85%, whereas the Waimihia andesite has a FeO_t/MgO value of 2.9 and a TiO_2 content of 1.56%. With the exception of the 1886 Tarawera and Rotokawau basalts, high-alumina basalts at rhyolitic centres in the Taupo Volcanic Zone have higher TiO_2 than basalts associated with calc-alkaline stratovolcanoes but even so, the Waimihia andesite still appears anomalous (Fig. 4c). An investigation of the andesite's origin is beyond the scope of this paper.

Sr isotope ratios have been measured in five samples (Fig. 4d) of andesite, rhyolite (Table 1) and streaky pumices. They have indistinguishable $^{87}Sr/^{86}Sr$ ratios of 0.70620–0.70626 (Ewart & Stipp 1968, reported a value of 0.7060 for 'Waimihia pumice'). These data lie towards the upper limit of values recorded from Taupo Volcanic Zone magmas. The value for the Waimihia andesite is particularly high in comparison with other Taupo andesites of similar SiO_2 and MgO contents or Rb/Sr ratios (Fig 4d).

Mineralogy and mineral compositions

All three Waimihia magma types have few phenocrysts. In particular, digestion of rhyolite pumice with HF acid yielded 1.3 to 2.7 wt% of crystals, while Walker (1981) estimated 3.3 wt% from crushing and panning, and Ewart (1963) 1.1 to 4.5 vol% from modal analyses. In the rhyolite, phenocrysts are dominantly plagioclase with minor orthopyroxene and traces of magnetite and ilmenite (usually as inclusions in orthopyroxene), and apatite (usually in plagioclase but also in orthopyroxene). A few samples contain the occasional augite and amphibole crystals but these are exceedingly rare. The rhyodacite has a lower crystal content than the rhyolite, and contains sparse plagioclase, orthopyroxene, magnetite and ilmenite in a clear vesicular glass. Andesite contains

Table 1. *Chemical compositions of Waimihia magmas*

Rock type / *Sample Number*	*Rhyolite average*[a]	*Rhyodacite P476/1*[b]	*Andesite P79A*[c]
Major element oxides[d]			
SiO_2	74.99 (19)[e]	70.93	58.87
TiO_2	0.24 (2)	0.56	1.56
Al_2O_3	13.36 (10)	14.04	15.63
Fe_2O_3	2.37 (12)	4.11	8.82
MnO	0.08 (2)	0.10	0.15
MgO	0.29 (5)	0.88	2.80
CaO	1.51 (3)	2.69	6.37
Na_2O	4.23 (10)	3.95	3.75
K_2O	2.87 (3)	2.45	1.30
P_2O_5	0.06 (1)	0.27	0.74
LOI	2.19 (25)	2.23	0.93
Trace elements[f]			
Ba	579 (7.5)	515	315
Rb	103 (1)	87	44.5
Sr	137 (3)	184	325
Pb	19 (1)	18	11
Th	13.5 (5)	11.5	5
U	3.0 (5)	2.5	2
Zr	242 (4)	216	124
Nb	8.5 (5)	8.5	5
Y	32 (1)	32	25
Ce	56 (1)	52	40
V	<1	28	101
Cr	<1	1	3
Cu	2 (0)	2	1
Zn	72 (1)	81	104
$^{87}Sr/^{86}Sr$[g]	0.70622 ± 6	0.70626 ± 3	0.70620 ± 4

a: Major elements: average of 13 analyses. Trace elements: average of 15 analyses.
b: Sample lodged in Research School of Earth Sciences, Australian National University, as 86–93 (pumice fragment), 86–98 (powder).
c: Sample lodged in Geology Department, University of Auckland as AU 39887 and in Research School of Earth Sciences, ANU, as 86–101.
d: XRF analyses, Department of Geology, University of Auckland. Analyses recalculated to 100% anhydrous with all iron expressed as Fe_2O_3.
e: numbers in brackets are sample standard deviation in the smallest reported units, e.g. for silica 74.99 ± 0.19 wt%.
f: XRF analyses, Department of Geology, Australian National University, analyst B. W. Chappell.
g: analyses by M. T. McCulloch, RSES, ANU. Rhyolite analysis for sample P470 (ANU: 86–97) (see Fig. 3d for further data).

plagioclase phenocrysts, augite, orthopyroxene and magnetite in a dark brown glassy to microcrystalline groundmass that contains swallowtail plagioclase laths.

Single pumices were crushed and hand-picked crystal separates were mounted in resin for microprobe analysis, along with polished thin sections of scoria. Mineral and glass analyses were obtained using the energy dispersive electron microprobe analyser at the Research School of Earth Sciences, Australian National University. Operating conditions were 3 nA beam current and 20 kV accelerating voltage. Data reduction procedures were those of Ware (1981). Representative analyses are given in Tables 2–4.

Plagioclase

In the rhyolite pumice plagioclase forms euhedral phenocrysts up to 3 mm. With few exceptions these have compositions of An_{29-49} with a distinct mode at An_{35-39} (Fig. 5); Or contents are 1–3% and they contain 0.1–0.3% FeO. They show a fine-scale oscillatory zonation with optically discernible wavelengths of less than a few microns. Ewart (1963, his Fig. 11) illustrates this complex pattern which demonstrates episodes of both crystal growth and resorption. Compositional evidence of zoning is less clear. Microprobe traverses were made over several phenocrysts, but no consistent pattern was revealed. Cores are typically more calcic than rims, but the least calcic portions of some crystals are at an intermediate position with centres and rims sharing the same composition. Interpreting these zoning patterns is fraught with geometrical problems because different crystals can be sectioned without exposing their true centres or in orientations that distort zoning patterns. Also, differences in nucleation times and growth rates between crystals in the same sample can cloud correlations of compositional zoning patterns.

Plagioclases in streaky pumice are mostly similar to those in the rhyolitic pumice, showing a strong mode at An_{36}. However one sample, P470A, (Fig. 5), contains complexly zoned, more calcic plagioclases (An_{43-75}) similar to phenocryst

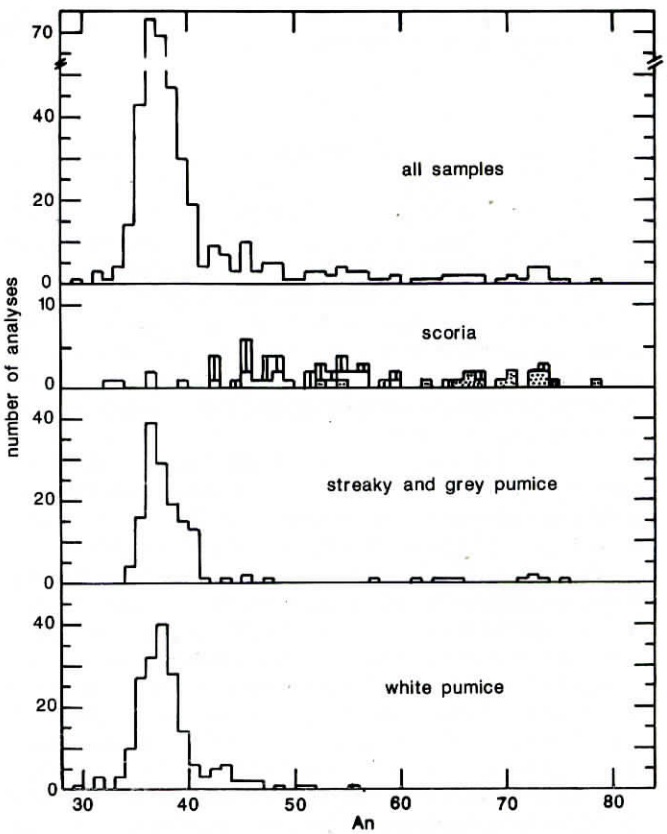

Fig. 5. Histogram of anorthite contents of plagioclase in white pumice, streaky and grey pumice, scoria, and all samples. The different patterns in the histogram for scoria identify different petrographic associations: shaded, phenocrysts enclosed by dark glass or microcrystalline groundmass; clear, phenocrysts enclosed by clear glass; striped, microphenocrysts.

Table 2. *Representative microprobe analyses of minerals and glass in rhyolitic magma*

Sample	P471A				IB	IB	IB	P475B	P470A
Material	plag	opx	mt	il	opx	cpx	hb	glass	apatite
SiO_2	58.87	49.83	0.28	0.12	50.20	51.32	43.26	75.91	0.00
TiO_2	0.00	0.00	14.11	47.37	0.00	0.00	2.52	0.05	0.00
Al_2O_3	26.16	0.73	1.85	0.21	0.72	1.03	9.06	13.38	0.00
FeO	0.15	30.78	76.54	47.02	30.58	13.82	17.03	1.66	0.97
MnO	0.00	1.85	0.85	1.20	1.77	0.56	0.30	0.00	0.00
MgO	0.00	14.97	0.94	1.34	15.42	12.47	11.63	0.24	0.53
CaO	7.78	1.21	0.00	0.00	1.24	19.20	10.49	1.25	53.65
Na_2O	7.07	0.00	0.00	0.00	0.00	0.00	1.82	4.69	0.32
K_2O	0.27	0.00	0.00	0.00	0.00	0.00	0.33	2.73	0.00
P_2O_5	0.00	0.00	0.00	0.00	0.00	0.00	0.00	0.08	41.78
Total	100.30	99.37	94.57	97.37	99.93	98.39	96.43	94.02[a]	97.25
No. oxygens	8	6	32	3	6	6	23		
Si	2.624	1.962	0.085	0.0031	1.960	1.979	6.572		
Ti	0.000	0.000	3.215	0.9096	0.000	0.047	0.289		
Al	1.374	0.034	0.661	0.0063	0.033	0.018	1.623		
Fe^{3+b}	—	0.043	8.741	0.1686	0.047	—	—		
Fe^{2+}	0.006	0.970	10.655	0.8355	0.952	0.446	2.163		
Mn	0.000	0.062	0.218	0.0260	0.059	0.018	0.038		
Mg	0.000	0.878	0.425	0.0510	0.898	0.716	2.633		
Ca	0.372	0.051	0.000	0.0000	0.052	0.793	1.708		
Na	0.611	0.000	0.000	0.0000	0.000	0.000	0.537		
K	0.015	0.000	0.000	0.0000	0.000	0.000	0.064		
P	0.000	0.000	0.000	0.0000	0.000	0.000	0.000		
Total cations	5.002	4.000	24.000	2.000	4.000	3.998	15.627		
Composition[c]	$An_{37.3}$ $Or_{1.5}$ $Ab_{61.2}$	$En_{43.8}$ $Wo_{2.5}$ $Fs_{53.7}$	$Usp_{42.7}$	$Ilm_{91.2}$	$En_{44.7}$ $Wo_{2.6}$ $Fs_{52.7}$	$En_{36.3}$ $Wo_{40.2}$ $Fs_{23.5}$	Mg# = 54.5		

[a] Glass analysis recalculated to 100%, total is of original analysis.
[b] Where given, Fe^{3+} calculated by stoichiometry.
[c] En = Mg/(Mg + Fe^{2+} + Fe^{3+} + Mn + Ca), Usp and Ilm according to Stormer (1983), Mg# = 100 Mg/(Mg + Fe^{2+} + Fe^{3+} + Mn).

compositions observed in the andesitic scoria. The maximum range in a single crystal is $An_{43.8}$ to $An_{71.2}$. The absence of this population from other streaky pumices is probably a sampling problem rather than real.

Plagioclase in scoria covers a wide range (An_{33-92}) but petrographic relations reveal a number of sub-populations. Phenocrysts and microphenocrysts surrounded by dark glass or a microcrystalline matrix are more calcic than about An_{52} and contain 0.6–0.7% FeO; they are normally zoned. A single crystal in sample P478D has compositions of An_{88-92} $Or_{0.5-0.0}$ and is considered to be a xenocryst (similar high-An plagioclases occur in an older Taupo high-alumina basalt; Wilson & Smith 1985). Clear highly-vesicular glass coats more sodic plagioclase phenocrysts of An_{32-60}. The most sodic varieties are up to several mm across and equant, like those in the rhyolite. The remainder are zoned in either reverse or normal fashion and the associated glass is rhyodacitic rather than rhyolitic (Table 3). Groundmass crystals are predominantly in the range An_{42-52}.

Orthopyroxene

Three compositional populations can be defined (Fig. 6). The first population is associated with the rhyolitic end member. In the rhyolite compositions range between En_{40} $Wo_{2.5}$ and En_{52} $Wo_{2.5}$ and the mean composition of about En_{44} $Wo_{2.5}$ is similar to that determined by wet chemical analysis of mineral separates by Ewart (1971). Normal zoning occurs in a few crystals but only over a few mol% En. Only in one phenocryst (in upper Waimihia sample P475B) was pronounced zoning found; here an $En_{53.4}$ $Wo_{2.3}$ core was smoothly zoned to an $En_{43.2}$ $Wo_{2.3}$ rim and this is responsible for the high Mg# tail in the rhyolite population in Fig. 6. There is no compositional variation with stratigraphic position. Streaky pumices contain a bimodal suite, with representatives of the rhyolitic assemblage and also more Mg-rich crystals of ca. En_{56} $Wo_{2.7}$ with Mg# $\approx$ 57 (Fig. 6) and detectable Ti (Table 3). The latter are also found among crystals surrounded by clear glass in scoria. The most Mg-rich orthopyroxenes in scoria are enclosed by dark glass or microcrystalline matrix and have Mg# $\approx$ 70 (En_{68} Wo_3).

Clinopyroxene

Two equilibrium phenocryst populations have been found (Tables 2 & 4) together with quench crystals and crystallites (Fig. 7). One population which clusters around $En_{42}Wo_{42}Fs_{16}$ has been found in the black scoria (in contact with dark glass and orthopyroxenes of $En_{69}Wo_3$) and in one streaky pumice.

Table 3. *Representative microprobe analyses of minerals and glass from rhyodacite magmas in streaky pumice and scoria*

Sample	P478A(scoria)				P476 (streaky pumice)			
Material	plag	opx	mt	il	opx	mt	il	glass
SiO_2	55.11	52.68	0.57	0.47	51.34	0.11	0.11	72.29
TiO_2	0.00	0.17	12.63	42.99	0.21	13.40	45.88	0.37
Al_2O_3	28.20	1.18	2.81	0.54	0.94	1.96	0.22	14.06
V_2O_3	0.00	0.00	0.18	0.00	0.00	0.00	0.00	0.00
FeO	0.42	20.59	75.00	48.20	24.99	75.48	46.66	2.61
MnO	0.00	0.83	0.62	0.70	11.26	0.73	0.95	0.00
MgO	0.28	22.63	2.21	3.05	19.35	1.31	2.09	0.62
CaO	10.71	1.37	0.00	0.00	1.26	0.00	0.00	2.42
Na_2O	5.04	0.00	0.00	0.00	0.00	0.00	0.00	4.81
K_2O	0.25	0.00	0.00	0.00	0.00	0.00	0.00	2.29
P_2O_5	0.00	0.00	0.00	0.00	0.00	0.00	0.00	0.53
Total	100.01	99.46	94.03	95.95	99.34	92.99	95.91	94.03[a]
No. oxygens	8	6	32	3	6	32	3	
Si	2.486	1.963	0.171	0.0119	1.960	0.034	0.0028	
Ti	0.000	0.005	2.847	0.8197	0.006	3.093	0.8868	
Al	1.499	0.052	0.993	0.061	0.042	0.709	0.0067	
V	—	0.000	0.043	0.0000	0.000	0.000	0.0000	
Fe^{3+b}	0.000	0.012	8.930	0.3209	0.026	9.039	0.2143	
Fe^{2+}	0.016	0.630	9.871	0.7011	0.772	10.336	0.7887	
Mn	0.000	0.026	0.157	0.0150	0.041	0.190	0.0207	
Mg	0.019	1.257	0.987	0.1153	1.101	0.599	0.0801	
Ca	0.517	0.055	0.000	0.0000	0.052	0.000	1.0000	
Na	0.441	0.000	0.000	0.0000	0.000	0.000	0.0000	
K	0.014	0.000	0.000	0.0000	0.000	0.000	0.0000	
P	0.000	0.000	0.000	0.0000	0.000	0.000	0.0000	
Total cations	4.992	4.000	24.000	2.0000	4.000	24.000	2.0000	
Composition[c]	$An_{53.2}$ $Or_{1.4}$ $Ab_{45.4}$	$En_{63.5}$ $Wo_{2.8}$ $Fs_{33.7}$	$Usp_{38.9}$	$Ilm_{82.5}$	$En_{55.3}$ $Wo_{2.6}$ $Fs_{42.1}$	$Usp_{40.7}$	$Ilm_{88.6}$	

[a] Glass analysis recalculated to 100%, total is of original analysis.
[b] Where given, Fe^{3+} calculated by stoichiometry.
[c] En = Mg/(Mg + Fe^{2+} + Fe^{3+} + Mn + Ca), Usp and Ilm according to Stormer (1983), Mg# = 100 Mg/(Mg + Fe^{2+} + Fe^{3+} + Mn).

The other population, at $En_{36}Wo_{41}Fs_{23}$, is defined by one crystal from one scoria sample and two crystals found in a cluster with orthopyroxene ($En_{45}Wo_{2.6}$), plagioclase (An_{41}) and hornblende (Mg# $\approx$53) in sample IB of white pumice from the Waimihia ignimbrite. The quench crystals are generally Ca-poor (Fig. 7), consistent with disequilibrium crystallization.

Magnetite

Three compositional populations can be defined (Fig. 8, Tables 2–4). In rhyolite pumices magnetite occurs as inclusions in orthopyroxene and, occasionally, plagioclase. These equant crystals are compositionally homogeneous and have an average composition of Usp_{43} (calculation method of Stormer 1983) (Tables 2–4). This population forms a well-defined group in the centre of a plot of the minor components (Al_2O_3 + V_2O_3), MgO and MnO (Fig. 8) (although the V_2O_3 contents of these magnetites are below the detection limit of the microprobe).

The second population of magnetites are found in streaky pumices and in scoria, where they or their host minerals are enclosed by clear glass. Compositions are in the range $Usp_{38.6-41.2}$ and these magnetites have higher MgO/MnO ratios (Fig. 8) than rhyolitic magnetites. The third magnetite population is only found in the scoria, occurring in the dark groundmass as discrete phenocrysts and as inclusions in pyroxenes. This population has Usp_{40-42} but can be easily distinguished from other populations by its much higher MgO/MnO ratio (*c.* 10; see Fig. 8) and V_2O_3 contents up to 0.5%.

Rhyolitic pumice studied by Ewart *et al.* (1975) gave similar magnetite compositions to those reported here for the white pumice population. Topping & Kohn (1973) and Kohn (1970) reported partial analyses of Waimihia magnetite crystal separates. The average composition had MgO/MnO = 1.73 and individual analyses gave $1.13 \leqslant \text{MgO/MnO} \leqslant 2.15$. This scatter suggests that their analysed material contained magnetites from more than one of the magnetite populations found in the present study.

Ilmenite

This has been found in white pumice, streaky pumice, and in dark scoria containing clear vesicular glass. Two compositional populations are recognized (Fig. 8, Tables 2 & 3). In white pumice, ilmenite ($Ilm_{91.45\pm0.79}$) occurs (with magnetite) as

Table 4. *Representative analyses of minerals in andesitic magma in scoria*

Sample	P478A				P478D
Material	plag	opx	cpx	mt	plag xenocryst
SiO_2	50.71	52.90	49.60	0.59	45.81
TiO_2	0.00	0.27	0.89	13.39	0.00
Al_2O_3	30.99	1.77	3.88	3.54	35.10
V_2O_3	0.00	0.00	0.00	0.27	0.00
FeO	0.64	17.74	10.19	73.44	0.46
MnO	0.00	0.43	0.22	0.44	0.00
MgO	0.17	24.71	14.01	3.42	0.20
CaO	14.20	1.51	19.02	0.00	18.27
Na_2O	3.20	0.00	0.00	0.00	0.97
K_2O	0.09	0.00	0.00	0.00	0.00
Total	100.00	99.34	98.87	95.08	100.81
No. oxygens	8	6	6	32	8
Si	2.313	1.944	1.884	0.173	2.096
Ti	0.000	0.007	0.025	2.949	0.000
Al	1.666	0.077	0.173	1.222	1.893
V	0.000	0.000	0.000	0.063	0.000
Fe^{3+a}	—	0.021	0.031	8.472	—
Fe^{2+}	0.024	0.525	0.292	9.518	0.018
Mn	0.000	0.013	0.007	0.109	0.000
Mg	0.011	1.354	0.792	1.493	0.013
Ca	0.694	0.059	0.773	0.000	0.896
Na	0.283	0.000	0.000	0.000	0.086
K	0.005	0.000	0.000	0.000	0.000
Total cations	4.998	4.000	4.000	24.000	5.001
Composition[b]	$An_{70.6}$ $Or_{0.6}$ $Ab_{28.8}$	$En_{68.7}$ $Wo_{3.0}$ $Fs_{28.3}$	$En_{41.8}$ $Wo_{40.8}$ $Fs_{17.4}$	$Usp_{40.7}$	$An_{91.3}$ $Or_{0.0}$ $Ab_{8.7}$

[a] Where given, Fe^{3+} calculated by stoichiometry.
[b] En = Mg/(Mg + Fe^{2+} + Fe^{3+} + Mn + Ca), Usp and Ilm according to Stormer (1983), Mg # = 100 Mg/(Mg + Fe^{2+} + Fe^{3+} + Mn).

inclusions in orthopyroxene and plagioclase. The crystals have no detectable zoning nor stratigraphically-related variations. These crystals have MgO/MnO ratios a little over 1.0 (Fig. 8) and minor Al_2O_3 (0–0.3%). Ewart *et al.* (1975) report similar ilmenite compositions. Members of this population are also found in streaky pumices (Fig. 8), but these and the mafic clasts also contain a more magnesian ilmenite (MgO/MnO = 2.5) of $Ilm_{82.5-88.6}$ occurring as crystals in orthopyroxene phenocrysts. The compositions of both magnetite and ilmenite inclusions correlate with that of their hosts. Thus the MgO/MnO ratios of the opaque phases correlates positively with the Mg # of orthopyroxene and the An content of plagioclase.

Apatite

An analysis of apatite hosted in orthopyroxene ($En_{46.5}Wo_{2.4}Fs_{51.1}$) from streaky pumice P470A is given in Table 2.

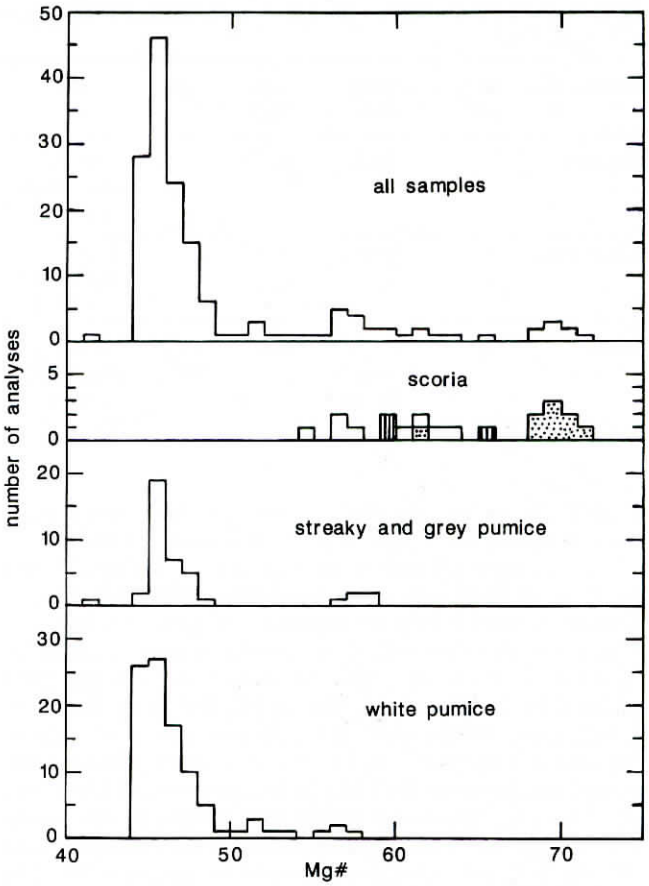

Fig. 6. Histogram of Mg # (= 100 Mg/(Mg + $Fe^{2+}Fe^{3+}$ + Mn)) of orthopyroxene in white pumice, streaky and grey pumice, scoria, and all samples. Patterns in scoria histogram as in Fig. 5.

Temperature and water content of Waimihia magmas

Correlations between whole rock composition, glass composition and phenocryst compositions in the Waimihia ejecta allow three magma types to be recognized (Table 5). These are homogeneous rhyolite, a compositionally somewhat variable rhyodacite and an andesite. To characterize all three magmas

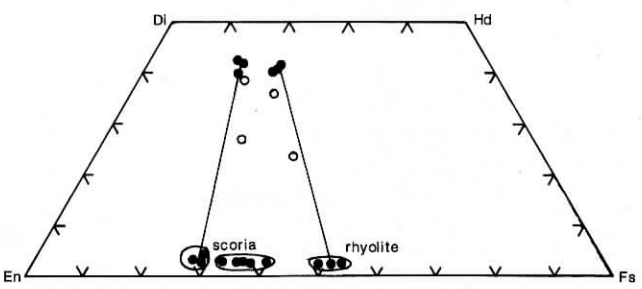

Fig. 7. Pyroxene quadrilateral showing compositions of clinopyroxenes, joined with tielines to co-existing orthopyroxenes, and representative orthopyroxenes in scoria (andesite and rhyodacite populations) and white pumice (rhyolite population). Open symbols identify crystals with quench morphologies.

Table 5. *Summary of magma characteristics, including average mineral compositions, estimated temperature, viscosity (Shaw 1972) and density (Mo* et al. *1982)*

Magma type	SiO_2 wt%	plag %An	opx Mg#	cpx	mt	il	T/°C	$\log_{10}$ (f_{O_2}bar)	H_2O %	kinematic viscosity $m^2\ s^{-1}$	density kgm^{-3}
Rhyolite	75	29–49	40–52	trace En_{36} Wo_{41}	Usp_{43} MgO/MnO ≈0.7–1.2	$Ilm_{91.5}$ MgO/Mn ≈1.0–1.5	830 ±30	−13.8 ± 1.0	4.3	46 (0.4 at 1100°C)	2200
Rhyodacite	71	approx 41–75	54–63	—	$Usp_{38.6-41.2}$ MgO/MnO ≈1.7–4	$Ilm_{82.5-88.6}$ MgO/MnO ≈2.1–4.0	860 −915	−12.7 to −11.2	3.7	24 at 860°C 8.1 at 915°C	2250
Andesite	59	52–79 (xenocrysts 88–92)	68–71	En_{42} Wo_{42}	Usp_{40-42} MgO/MnO ≈10	—	1100	—	2	0.14	2425

further, thermodynamic methods are used to estimate magmatic temperature, oxygen fugacity and water contents.

Temperatures (T) and oxygen fugacities (f_{O_2}) of equilibrium Fe–Ti oxide pairs were calculated using end-member calculations of Stormer (1983), the equations of Spencer & Lindsley (1981) and the thermodynamic constants recommended by Anderson & Lindsley (1985). Magnetite and ilmenite pairs (defined by consistent Mg/Mn ratios, following Bacon & Hirschmann 1988) yield the temperatures and oxygen fugacities plotted in Fig. 9. The rhyolites (white pumice) show a trend which crosses the FMQ buffer curve around 820°C and 10^{-14} bars f_{O_2}. This trend mimics that defined by opx ± cpx-bearing rhyolites studied by Carmichael (1967), who proposed that the T–f_{O_2} relationship was defined by an opx buffer. The same trend was documented in Taupo rhyolites by Ewart *et al.* (1975).

The magnetite and ilmenite compositions and resulting oxide temperatures in the rhyolites are unrelated to stratigraphic position. The means and sample standard deviations are $X_{usp} = 0.43006 \pm 0.00691$ ($n = 66$) and $X_{ilm} = 0.91447 \pm 0.00790$ ($n = 37$). The uncertainties in mineral compositions lead to uncertainties in T of 30–50 °C and up to a factor of 10 in f_{O_2}. T–f_{O_2}/X_{usp}–X_{ilm} relationships defining the geothermometer and geooxybarometer are such that a random selection of magnetite and ilmenite compositions yields a T–f_{O_2} trend identical to that shown in Fig. 9. So the plotted array of rhyolite data need not define a real magmatic trend. (Another illustration of this effect is clear in the results published by d'Arco *et al.* (1981, their fig. 3).) The variation among the rhyolites shown in Fig. 9 is at the limit of the method's expected uncertainties and T is estimated as 830 ± 30 °C.

Rhyodacite oxide pairs give higher temperatures and oxygen fugacities than the rhyolite (Fig. 9) and are compositionally distinct from each other in minor element contents (Fig. 8) and in X_{usp} and X_{ilm}. The differences in T and f_{O_2} between these samples and the rhyolites are thus taken to be real. Notice that T increases with increasing MgO/MnO ratios of the oxides (Fig. 8). The magnetite–ilmenite geothermometer is usually regarded as the most reliable, but others can be applied to the Waimihia rocks. The orthopyroxene–ilmenite thermometer of Bishop (1980) gives temperature estimates for the rhyolites and rhyodacites which are consistently some 100 °C higher than

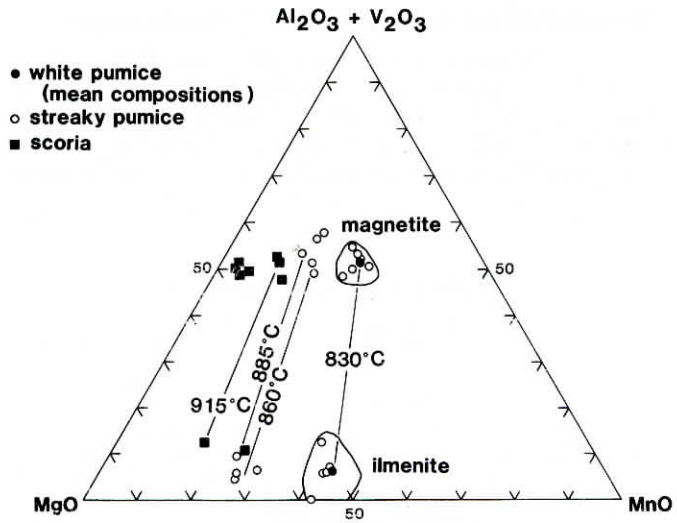

Fig. 8. Minor element diagram of magnetite and ilmenite analyses. Filled circles, average compositions in white pumice; open circles, streaky and grey pumice; filled squares, scoria. Rhyolitic populations are enclosed and are present along with rhyodacitic population in streaky and grey pumices. Temperatures calculated from co-existing oxides linked by tielines.

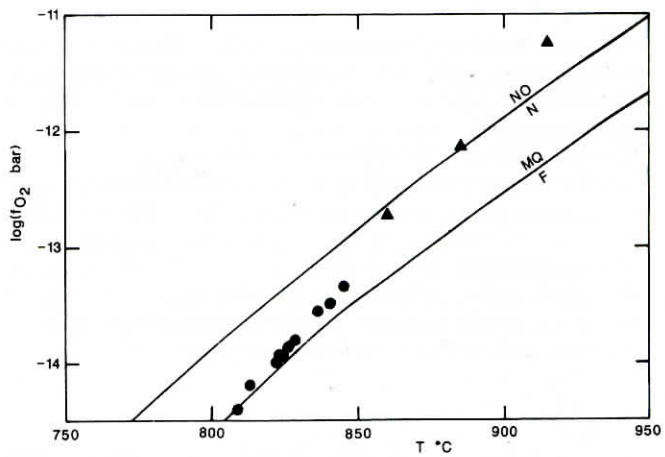

Fig. 9. T–f_{O_2} diagram for all co-existing oxide pairs. Circles, rhyolite; triangles, rhyodacite.

those obtained from co-existing oxides. This systematic difference reflects uncertainties in both thermometers but points to equilibrium between all three phases.

The two pyroxene thermometer of Lindsley (1983) has been applied to the single sample of cpx + opx bearing rhyolite (from ignimbrite sample IB see Table 2) and to andesitic scoria. The rhyolite gives a temperature of 900 °C and the andesite 1100 °C. The equations of French & Cameron (1981) indicate a plag + cpx cotectic liquidus temperature of 1090 °C for andesite P79A, assuming 2% water (see later). Nielsen & Dungan (1983) have demonstrated that the partitioning of Al between melt and Fe^{3+}-bearing spinel provides a geothermometer, at least in the approximate range 1100–1200 °C. The four magnetites which define the andesitic population (Fig. 8) have $3.85 \pm 0.18\%$ Al_2O_3 and in conjunction with the alumina content of andesite scoria P79A (Table 1) yield a 1-atmosphere equilibration temperature of 1094 °C. It is encouraging that three very different methods give identical results for the andesite. Preferred temperatures are thus 830 ± 30 °C for rhyolite, 860–915 °C for rhyodacites, and 1100 °C for the andesite (Table 3).

Glass inclusion analyses (Dunbar *et al.* 1989*b*) on rhyolite from the 1800 years BP Taupo eruption give a water content of 4.3 ± 0.5 wt%. As the Taupo and Waimihia rhyolites have virtually identical chemistries, mineralogies, T and f_{O_2} it is reasonable to infer the same water content for the Waimihia magma.

The water content of the andesite can be estimated using the method of Merzbacher & Eggler (1984). This technique takes advantage of the fact that the composition of a liquid which co-exists with orthopyroxene, augite and plagioclase is virtually independent of T and P but not X_{H_2O}. Since the Waimihia andesite contains these three minerals as phenocrysts, the bulk composition is used to approximate the near-liquidus melt composition of these crystal-poor rocks. This method indicates an original water content of 2%.

Interpretation

In this section we integrate the volcanological, chemical and mineralogical results into a consistent model of the magmatic and eruptive processes leading to formation of the Waimihia deposits. Critical aspects of the erupted magmas are:

(1) on variation diagrams all rock compositions plot on a straight line joining the most mafic (andesitic) and silicic (rhyolitic) rocks (Fig. 4);

(2) chemical hybridization of andesite and rhyolite has produced rhyodacites containing equilibrium phenocrysts, a hybrid glass, and xenocrysts inherited from the end-members;

(3) mechanical mixing of rhyodacite and rhyolite produced streaky pumice, and mechanical mixing of rhyodacite and andesite produced those scoria clasts that are not pure andesite;

(4) the proportions of streaky pumice and scoria are stratigraphically-related (Fig. 3). Scoria is most common in the upper parts of the second plinian phase of the eruption (upper Waimihia), but streaky pumice (and hence rhyodacite) is most abundant at the base of this unit. Thus the most mafic bulk composition of the Waimihia is at the base of the upper fall deposit but the maximum abundance of the most mafic clasts occurs 2/3 of the way up through this unit.

Magma mixing during chamber evacuation: origin of banded pumice

The stratigraphic variation in magma composition in the Waimihia deposit is similar to that expected from the withdrawal of magma from a three-layer stratified chamber. The gravitationally stable arrangement of Waimihia magmas would have been rhyolite underlain by rhyodacite underlain by andesite. The range of temperatures and mineral compositions associated with the rhyodacite (Figs 5 to 9) suggests a range of hybrid magma compositions, and implies the presence of compositional and thermal gradients across the rhyodacite layer separating the rhyolite from the andesite. An eruption that taps such a stratified chamber from its roof will preferentially tap the layers(s) of lowest density, with the extent to which dense layers are tapped being governed by the thickness of overlying layers and the withdrawal rate. A thick capping layer and low discharge rate favour selective withdrawal of the uppermost layer, whilst a thin cap and high discharge rate favour the lower layers being tapped (Blake & Ivey 1986). Fluid dynamic instabilities cause the magmas to be mingled, forming streaky mixtures, whilst travelling in the conduit (Koyaguchi 1985; Blake & Campbell 1986; Freundt & Tait 1986).

During the lower Waimihia eruption, a uniform eruption rate of *c.* $8 \times 10^8\,kg\,s^{-1}$ ($\approx 3.6 \times 10^5\,m^3\,s^{-1}$) is implied by the

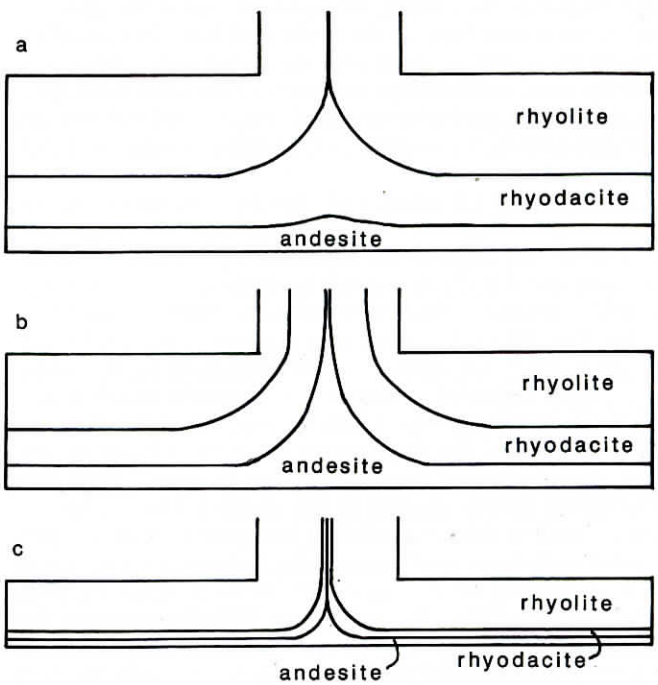

Fig. 10. Schematic stages of chamber evacuation during the Waimihia eruption. (**a**) At the beginning of the lower Waimihia eruption the rhyolite is too thick to allow significant tapping of rhyodacite or andesite. (**b**) During the last part of the lower Waimihia and first parts of the upper Waimihia, sufficient rhyolite has been evacuated for rhyodacite to gain access to the outlet, andesite is just being tapped. (**c**) At the close of the upper Waimihia eruption, andesite is still barely being tapped but most of the rhyodacite has been extracted and, therefore, provides a smaller proportion of the ejected magmas than previously, despite being closer to the outlet.

pattern of clast dispersal and the lack of vertical size grading. If this reflects a constant rate of magma removal from the chamber, then the increase in the proportion of rhyodacite through this unit is accounted for solely by the progressive thinning of the rhyolite layer allowing rhyodacite to be entrained into the venting rhyolite (Fig. 10a,b). Approximating the rhyodacite as an homogenous layer of density 2250 kgm^{-3} (Table 5), then the equations of Blake and Ivey (1986) indicate that the rhyolite layer must have been less than about 250 m thick for significant entrainment of rhyodacite (i.e. greater than 2.5% rhyodacite in the output). This condition was achieved near the end of the lower Waimihia phase of the eruption (Fig. 3).

The lowest part of the upper Waimihia contains a greater proportion of mafic magmas (grey and black clasts) than does the uppermost part of the lower Waimihia. One possible explanation is that the opening phase of the upper Waimihia involved a higher evacuation rate than the closing phase of the lower Waimihia. However, the grain-size characteristics of the two fall units are so similar as to imply insignificant differences in discharge rate. On the other hand, this need not imply equal evacuation rates because the fragmentation level in the conduit may migrate up or down to accommodate imbalances in the rates of entry to and exit from the conduit, and the relationships between discharge and evacuation rates are unknown. Another possible explanation, which we prefer, is a change in the relative positions of the chamber outlet and the rhyolite/rhyodacite interface. If the evacuation rates were indeed the same in the two eruptions, then during the upper Waimihia the chamber outlet must have been closer to the interface. This could be caused by a shift in outlet position to one lower down in a sloping roof. Alternatively, the same outlet could have been used in both eruptions but structural readjustment of the chamber roof in the intervening period could have brought the outlet closer to the interface.

Explanations for subsequent changes in magma composition are less ambiguous. The decreasing rhyodacite component and increasing andesite are explicable by the evacuation of rhyolite and rhyodacite causing progressive decreases in the available amount of rhyodacite and in the depth to the andesite layer (Fig. 10b,c). The conditions required to entrain a small amount ($\ll 2.5\%$) of andesite, as seen throughout the Waimihia, are difficult to quantify. Laboratory experiments of withdrawal from two-layer chambers (Jirka & Katavola 1979; Blake & Ivey 1986) show that the composition of the effluent at very low concentrations of lower layer is very sensitive to the size of the diffuse density gradient at the interface (the interface is never infinitely thin). Nonetheless, in a given case, the proportion of lower layer is still increased by increasing the discharge rate or thinning of the upper layer (Jirka & Katavola 1979; Blake & Ivey 1986). Throughout the Waimihia eruption the combined thickness of rhyolite and rhyodacite must have been greater than the critical thickness at which 2.5% andesite could be entrained. For the hypothetical system of Waimihia rhyolite overlying andesite (properties in Table 5), and eruption at $3.6 \times 10^5 m^3 s^{-1}$ a critical thickness of 150 m is calculated. The same calculation assuming a rhyodacite upper layer gives a very similar result because the density of the rhyodacite is much closer to that of the rhyolite and because entrainment at such a high discharge takes place in a high Reynolds number regime, where viscosity is unimportant. Calculations of critical withdrawal layer thickness thus enable us to state that the rhyolite layer was less than 250 m thick for at least the last half of the Waimihia eruption (i.e. above the *c.* 3 m level in the logged section) and that the combined thickness of rhyolite and rhyodacite was always greater than 150 m. Selective withdrawal of rhyodacite at the expense of denser andesite accounts for the peak in rhyodacite production preceding that of the andesite.

In the final stages of the eruption the proportions of rhyodacite and andesite decrease. This could reflect a decreasing eruption rate (cf. Vesuvius AD 79; Sigurdsson *et al.* 1990), but available evidence suggests that the rate remained uniform, with simply a proportion of the material being erupted as ignimbrite. Another possibility is that the total volumes of rhyodacite and andesite were such that they had been almost entirely evacuated during earlier phases of the eruption (Fig. 10c). One supporting piece of evidence for this view is that in the Taupo eruption, which occurred only 1500 years later from the same vent area, the only trace of non-rhyolitic magma we have found is a *c.* 1 cm diameter andesite inclusion in a pumice from the Taupo plinian fall deposit. This inclusion has the same characteristic major-element composition as the Waimihia andesite (e.g. $SiO_2 = 59.13\%$, $TiO_2 = 1.51\%$, $P_2O_5 = 0.71\%$ (C.J.N.W. & I.E.M.S., unpub. data); cf. Table 1). No other signs of Waimihia-type andesite or rhyodacite have been found as lithic clasts or juvenile material in the 1800 yr BP deposits, suggesting that they were entirely evacuated during the Waimihia eruption.

Magma chamber shape

The areal dimensions of the Waimihia chamber can be constrained, albeit loosely, from the volume of magma erupted and the limits which the calculations of critical withdrawal layer thickness place on the depth of the rhyolite layer. It was estimated that approximately half-way through the Waimihia activity, at the moment rhyodacite constituted 2.5% of the ejecta, the rhyolite was *c.* 250 m thick. By the end of the eruption a further *c.* 3.5 km^3 of rhyolite had been erupted, but without reducing the thickness of rhyolite to less than 150 m. The area of a 100 m thick layer of the quoted volume is equivalent to a circle of radius 3.3 km (or 2.4 km using Pyle's method of volume estimation), suggesting a slab-like geometry for the rhyolite magma chamber. A consequence of this shape is that much more heat will be lost from the magma through its roof than through its walls. Convection in the chamber would have been controlled by cooling at the roof more than by convective fractionation induced by sidewall crystallization. Such a rhyolite 'sill' will tend to be kept homogenized by turbulent convection rather than become zoned by convective fractionation (de Silva 1991). This provides an explanation for the mineralogical and compositional homogeneity of the Waimihia rhyolite. As these traits are shared by all documented post-22 ka Taupo rhyolites (Dunbar *et al.* 1989*a*) we propose that these magmas were also stored in flat magma chambers.

Magma mixing during chamber replenishment: origin of rhyodacite

The fluid dynamics of withdrawal and transport from a stratified chamber account for the mechanical mixing that produced streaky pumice and heterogeneous scoria. The existence of the stratified chamber implies that rhyodacite was produced in an earlier magma mixing event within the chamber. This is consistent with the presence of equilibrium assemblages of equant phenocrysts in the rhyodacite magma; they could not

have grown during the short time during travel between the chamber and the fragmentation level in the conduit.

The energy to cause mixing between rhyolite and andesite could have come from the forceful injection of one magma into the other. There are two possibilities: recharge of a rhyolite chamber with andesite, or *vice versa.* The dominance of rhyolitic magma at Taupo, and the absence of andesite in the first erupted Waimihia magma indicates that andesite was the input magma. For slow inputs, the dense andesite magma will spread out as a 'lava flow' on the chamber floor and exchange heat with the light magma across a sharp double-diffusive interface (Huppert & Sparks 1980). Due to its high viscosity a thin layer of rhyolite would be trapped beneath the advancing andesite. This is gravitationally unstable and plumes of rhyolite would eventually rise into the andesite, to be hybridized by turbulent convection in the andesite 'lava flow'. Mixing might also occur at the front of the intrusion, as seen in laboratory experiments by Didden & Maxworth (1982). These processes would produce a layer of hybrid rhyodacite sandwiched between less dense rhyolite and denser uncontaminated andesite.

Alternatively, if the input is rapid, a fountain of dense magma is injected into the lighter magma and mixing can proceed within the fountain if the flow is sufficiently energetic (Campbell & Turner 1985). The hybrid magmas fall back around the input site and flow out to generate a stably stratified region at the appropriate density level in the chamber (Fig. 11). Campbell & Turner (1985, 1986) have identified the conditions under which a fountain will mix with its surrounding environment so the admissibility of this mixing mechanism can be assessed by applying their results. The important parameters are the kinematic viscosities of the input and reservoir magmas, ν_i and ν_r, the speed of the injected magma, w, and the width of the inlet orifice, d. Campbell & Turner showed that the input Reynolds number $Re_i = wd/\nu_i$ and the viscosity ratio ν_r/ν_i determine the dynamical interaction between the fountain and its environment. When $\nu_r \approx \nu_i$ mixing is efficient for $Re_i > 400$ but is absent for $Re_i < 30$. When $\nu_r \gg \nu_i$ significant mixing takes place when $Re_i > 70\,\nu_r/\nu_i$ but when $Re_i < 7\,\nu_r/\nu_i$ there is no mixing.

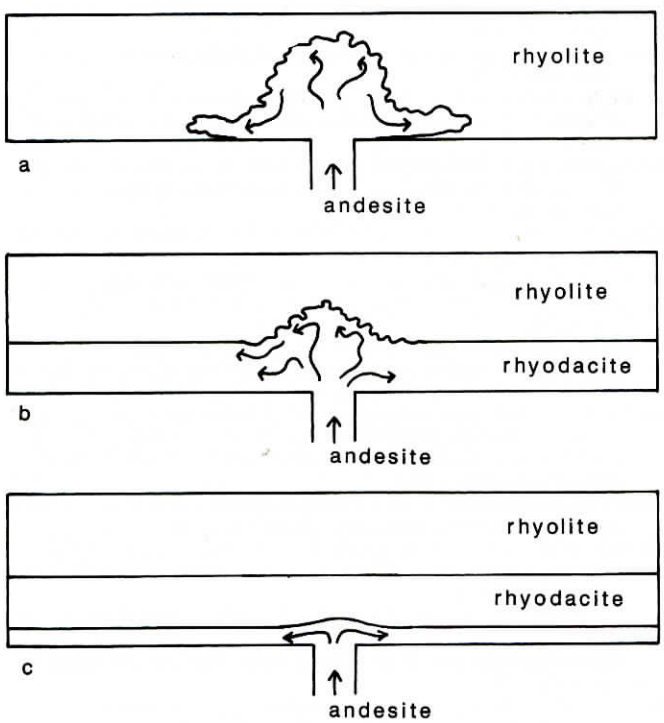

Fig. 11. Schematic development of the Waimihia magma chamber during injection of andesite magma. **(a)** Andesite fountains vigorously into the rhyolite chamber floor and spreads out to occupy the base of the chamber. **(b)** Continued input and mixing establishes a zoned rhyodacite layer. **(c)** As the andesite input rate wanes, a fountain cannot be sustained and andesite is emplaced beneath the rhyodacite without any mixing occurring.

To calculate the input Reynolds number w is first expressed as a function of ν_i, d and the pressure gradient which drives the flow. We assume the andesite is driven upwards by its buoyancy relative to the crustal rocks through which it passes. The magma speed is then dependent on the parameter $G = g\,(\rho_c - \rho_i)/\rho_i$ where g is the gravitational acceleration and $\rho_c - \rho_i$ is the density difference between crust and input magma. A crustal density of 2725 kg m^{-3} is assumed in the following calculations. At $Re_i > 2000$, $w = (Gd/f)^{1/2}$ where f is a friction coefficient between 0.01 and 0.06, the exact value depending on Re_i and the roughness of the conduit walls. A representative value for f is 0.03. At $Re_i < 2000$, $w = Gd^2/24\,\nu_i$ (in a pipe feeder) or $w = Gd^2/12\,\nu_i$ (in a fissure).

The equations allow the critical input Reynolds number and the requisite minimum conduit size and recharge rate for mixing to be calculated (Table 6). As the viscosity of rhyolite is sensitive to temperature, the calculations examine the cases of ambient temperature (830 °C) and the extreme case of superheating to the temperature of the andesite (1100 °C). The lower the viscosity (i.e. higher temperature) the lower the input rate required to achieve hybridization. For rhyolite at 830 °C the minimum recharge rates are very large, and are similar to eruption rates associated with plinian eruptions of several cubic kilometres of silicic magma (Carey & Sigurdsson 1989, and the Waimihia eruptions themselves). High discharge rate eruptions of andesite include Soufrière (St Vincent) 1979, the 9.5 ka Natsuzaka eruption of Towada, and Hekla 1970, for which eruption rates were 1.3×10^4, 1.4×10^4 and 3.3×10^3 m^3 s^{-1} respectively (Carey & Sigurdsson 1989; Cas & Wright 1987). These rates are insufficient to cause mixing with rhyolite at 830 °C.

It is inevitable that the rhyolite would be heated by the replenishing magma. Efficient heat transfer from a turbulent fountain would lower the viscosity of the rhyolite making it easier for the two magmas to mix. Recharge rates in the order of several hundred m^3 s^{-1} would then be able to cause mixing (Table 6). These conditions are met by the transport rates mentioned for the three eruptions above which were comparable in size to the volume of andesite involved in the Waimihia eruption (0.16 km^3). Thus if the rhyodacite was formed by fountain mixing in the Waimihia magma chamber, then this probably involved efficient heating of the rhyolite entrained in the mixing zone and comparatively large recharge rates (of the order of hundreds to thousands of m^3 s^{-1}). A period of lower recharge rate in which mixing did not occur would have allowed the uncontaminated andesite layer to be established at the base of the chamber (Fig. 11c).

Conclusions

The Waimihia pumice deposit provides information on the eruption conditions, magma compositions and magmatic

Table 6. *Conditions required to allow mixing during injection of andesite into rhyolite*

	temperature of rhyolite	
	830°C	1100°C
viscosity ratio, ν_r/ν_i	326	2.9
criterion for mixing	$Re_i > 2.3 \times 10^4$	$Re_i > 400$
minimum inlet size, d/m	63	*c.* 5
minimum input rate (pipe feeder)/$m^3\ s^{-1}$	1.6×10^5	235
minimum input rate (dyke)/$m^2\ s^{-1}$	3200	56

processes involved in one of the largest Holocene eruptions at Taupo volcano. Two plinian episodes were involved, the second included the emplacement of a small non-welded ignimbrite. Uniform discharge rates of *c.* 8×10^8 kg s^{-1} ($3.6 \times 10^5\ m^3\ s^{-1}$) are estimated for both Waimihia fall units. The fall deposits represent $<7.2\ km^3$ and the ignimbrite *c.* $0.3\ km^3$ of magma. Crystal-poor rhyolite pumice that is close in composition, mineralogy and iron-titanium oxide temperature to other post-22 ka Taupo rhyolites is the dominant rock type. Unlike other post-22 ka eruptions, however, the Waimihia deposits contain a medium-K tholeiitic andesite which occurs as rather dense scoriaceous clasts. Also hybridization has produced rhyodacites that occur mostly as streaks in banded pumice with rhyolite and also as grey pumice. The total erupted volumes of magmas are *c.* $7.0\ km^3$ rhyolite, $0.55\ km^3$ rhyodacite and $0.02\ km^3$ andesite, while if the rhyodacite is unmixed into its end-member components, there were $7.4\ km^3$ of rhyolite and $0.16\ km^3$ of andesite.

There were two episodes of magma mixing. First, andesite and rhyolite were hybridized within the magma chamber to form rhyodacite by andesite fountaining into the base of the rhyolite. This produced a three-layered chamber, with rhyolite overlying rhyodacite overlying andesite (Fig. 11). Second, mixing occurred when the magmas were travelling from the chamber to the surface. This produced banded pumice and occasional clasts of intricately mixed andesite/rhyodacite. Stratigraphic variation in the proportions of rhyolite, rhyodacite and andesite reflect the history of chamber evacuation (Fig. 10). Of the two plinian layers the upper Waimihia contains more of the mafic magmas. The proportion of rhyodacite increases upwards in the lower Waimihia layer as progressive withdrawal of rhyolite allowed increased access of the rhyodacite to the eruption conduit. The first magma erupted in the upper Waimihia contains more than five times as much rhyodacite as the last lower Waimihia magma. Given similar discharge rates, this is interpreted to reflect a repositioning of the outlet or chamber roof with respect to the rhyolite/rhyodacite interface in the chamber during the short interval between the two plinian phases. The proportion of rhyodacite decreases upwards in the upper Waimihia, whilst andesite is most abundant two thirds of the way up through this layer. The sequential appearance of denser magmas is explained by selective withdrawal from a stratified chamber. Calculations indicate that the rhyolite layer was about 250 m thick when rhyodacite was first tapped in significant quantities (i.e. 2.5% of the ejecta at that point in time), and that this layer was no less than 150 m thick at the end of the eruption. From this, it is inferred that the erupted volume of rhyolite was held in a broad sill-like chamber. This geometry favours heat transfer through the roof rather than through the walls of the chamber, promoting turbulent thermal convection which will inhibit the generation of compositional zoning by sidewall crystallization, thus accounting for the homogeneity of rhyolites in the Waimihia (in particular) and other Taupo rhyolites in general (e.g. Dunbar *et al.* 1989*a*).

We greatly appreciate the efforts of M. McCulloch and B. Chappell in obtaining isotope and trace element analyses. S.B. is grateful for N. G. Ware's help and instruction in using the microprobe, and the Australian National University's contribution to fieldwork expenses. C.J.N.W. thanks the Royal Society for financial support. We are pleased to acknowledge the helpful review comments of J. A. Gamble and an anonymous referee.

References

Anderson, D. J. & Lindsley, D. H. 1985. New (and final) models for the Ti-magnetite/ilmenite geothermometer and oxygen barometer. *Eos, Transactions American Geophysical Union,* **66,** 416.

Bacon, C. R. & Hirschmann, M. M. 1988. Mg/Mn partitioning as a test for equilibrium between coexisting Fe-Ti oxides. *American Mineralogist,* **73,** 57–61.

Bishop, F. C. 1980. The distribution of Fe^{2+} and Mg between coexisting ilmenite and pyroxene with applications to geothermometry. *American Journal of Science,* **280,** 46–77.

Blake, S. & Campbell, I. H. 1986. The dynamics of magma mixing during flow in volcanic conduits. *Contributions to Mineralogy and Petrology,* **94,** 72–81.

Blake, S. & Ivey, G. N. 1986. Magma mixing and the dynamics of withdrawal from stratified reservoirs. *Journal of Volcanology and Geothermal Research,* **27,** 153–178.

Campbell, I. H. & Turner, J. S. 1985. Turbulent mixing between fluids with different viscosities. *Nature,* **313,** 39–42.

—— 1986. The influence of viscosity on fountains in magma chambers. *Journal of Petrology,* **27,** 1–30.

Carey, S. & Sigurdsson, H. 1989. The intensity of plinian eruptions. *Bulletin of Volcanology,* **51,** 28–40.

Carey, S. & Sparks, R. S. J. 1986. Quantitative models of fallout and dispersal of tephra from volcanic eruption columns. *Bulletin of Volcanology,* **48,** 109–125.

Carmichael, I. S. E. 1967. The iron-titanium oxides of salic volcanic rocks and their associated ferromagnesian silicates. *Contributions to Mineralogy and Petrology,* **14,** 36–64.

Cas, R. A. F. & Wright, J. V. 1987. *Volcanic Successions Modern and Ancient.* Allen and Unwin, London.

Cole, J. W. 1979. *Chemical analyses of lavas and ignimbrites of the Taupo Volcanic Zone.* Victoria University of Wellington, Geology Department, Publication Number **13.**

d'Arco, P., Maury, R. C. & Westercamp, D. 1981. Geothermometry and geobarometry of a cummingtonite-bearing dacite from Martinique, Lesser Antilles. *Contributions to Mineralogy and Petrology,* **77,** 177–184.

de Silva, S. L. 1991. Styles of zoning in Central Andean ignimbrites—insights into magma chamber processes. *In:* Harmon, R. S. & Rapela, C. (eds) *Andean Magmatism and its Tectonic Setting.* Geological Society of America Special Paper **265** (in press).

Didden, N. & Maxworthy, T. 1982. The viscous spreading of plane and axisymmetric gravity currents. *Journal of Fluid Mechanics,* **121,** 27–42.

Dunbar, N. W., Kyle, P. R. & Wilson, C. J. N. 1989*a*. Evidence for limited zonation in silicic magma systems, Taupo Volcanic Zone, New Zealand. *Geology,* **17,** 234–236.

——, Hervig, R. L. & Kyle, P. R. 1989*b*. Determination of pre-eruptive H_2O, F and Cl contents of silicic magmas using melt inclusions: examples from Taupo volcanic center, New Zealand. *Bulletin of Volcanology,* **51,** 177–184.

Ewart, A. 1963. Petrology and petrogenesis of the Quaternary pumice ash in the Taupo area, New Zealand. *Journal of Petrology,* **4,** 392–431.

—— 1971. Notes on the chemistry of ferromagnesian phenocrysts from selected volcanic rocks, Central Volcanic Region. *New Zealand Journal of Geology and Geophysics,* **14,** 323–340.

—— & Stipp, J. J. 1968. Petrogenesis of the volcanic rocks of the Central North Island, New Zealand, as indicated by a study of $^{87}Sr/^{86}Sr$ ratios, and Sr, Rb, K, U, and Th abundances. *Geochimica et Cosmochimica Acta,* **32,** 699–735.

——, Hildreth, W. & Carmichael, I. S. E. 1975. Quaternary acid magma in New Zealand. *Contributions to Mineralogy and Petrology,* **51,** 1–27.

FRENCH, W. J. & CAMERON, E. P. 1981. Calculation of the temperatures of crystallization of silicates from basaltic melts. *Mineralogical Magazine,* **44,** 19–26.

FREUNDT, A. & TAIT, S. R. 1986. The entrainment of high-viscosity magma into low-viscosity magma in eruption conduits. *Bulletin of Volcanology,* **48,** 325–340.

FROGGATT, P. C. 1982. *A study of some aspects of volcanic history of the Lake Taupo area, North Island, New Zealand.* PhD thesis, Victoria University of Wellington, New Zealand.

—— & LOWE, D. J. 1990. A review of late Quaternary silicic and some other tephra formations from New Zealand: their stratigraphy, nomenclature, distribution, volume, and age. *New Zealand Journal of Geology and Geophysics,* **33,** 89–109.

GAMBLE, J. A., SMITH, I. E. M., GRAHAM, I. J., KIKELAAR, B. P., COLE, J. W., HOUGHTON, B. F. & WILSON, C. J. N. 1990. The petrology, phase relations and tectonic setting of basalts from the Taupo Volcanic Zone, New Zealand and the Kermadec Island Arc-Havre Trough, SW Pacific. *Journal of Volcanology and Geothermal Research,* **43,** 253–270.

GILL, J. B. 1981. *Orogenic Andesites and Plate Tectonics.* Springer-Verlag, Berlin.

GRAHAM, I. J. & HACKETT, W. R. 1987. Petrology of calc-alkaline lavas from Ruapehu volcano and related vents, Taupo Volcanic Zone, New Zealand. *Journal of Petrology,* **28,** 531–567.

—— & WORTHINGTON, T. J. 1988. Petrogenesis of Tauhara dacite (Taupo Volcanic Zone, New Zealand)—evidence for magma mixing between high-alumina andesite and rhyolite. *Journal of Volcanology and Geothermal Research,* **35,** 279–294.

HEALY, J., VUCETICH, C. G. & PULLAR, W. A. 1964. *Stratigraphy and chronology of Late Quaternary volcanic ash in Taupo, Rotorua and Gisborne Districts.* New Zealand Geological Survey Bulletin **73.**

HILDRETH, W. 1981. Gradients in silicic magma chambers: implications for lithospheric magmatism. *Journal of Geophysical Research,* **86,** 10153–10192.

HUPPERT, H. E. & SPARKS, R. S. J. 1980. The fluid dynamics of a basaltic magma chamber replenished by influx of hot, dense, ultrabasic magma. *Contributions to Mineralogy and Petrology,* **75,** 279–289.

JIRKA, G. H. & KATAVOLA, D. S. 1979. Supercritical withdrawal from two-layered fluid systems. Part 2: Three-dimensional flow into a round intake. *Journal of Hydraulic Research,* **17,** 53–62.

KOHN, B. P. 1970. Identification of New Zealand tephra-layers by emission spectrographic analysis of their titanomagnetites. *Lithos,* **3,** 361–368.

KOYAGUCHI, T. 1985. Magma mixing in a conduit. *Journal of Volcanology and Geothermal Research,* **25,** 365–369.

LINDSLEY, D. H. 1983. Pyroxene thermometry. *American Mineralogist,* **68,** 477–493.

MERZBACHER, C. & EGGLER, D. H. 1984. A magmatic geohygrometer: application to Mount St. Helens and other dacitic magmas. *Geology,* **12,** 587–590.

MO, X., CARMICHAEL, I. S. E., RIVERS, M. & STEBBINS, J. 1982. The partial molar volume of Fe_2O_3 in multicomponent silicate liquids and the pressure dependence of oxygen fugacity in magmas. *Mineralogical Magazine,* **45,** 237–245.

NIELSEN, R. L. & DUNGAN, M. A. 1983. Low pressure mineral-melt equilibria in natural anhydrous mafic systems. *Contributions to Mineralogy and Petrology,* **84,** 310–326.

PYLE, D. M. 1989. The thickness, volume and grainsize of tephra fall deposits. *Bulletin of Volcanology,* **51,** 1–15.

SHAW, H. R. 1972. Viscosities of magmatic silicate liquids: an empirical method of prediction. *American Journal of Science,* **272,** 870–893.

SIGURDSSON, H., CORNELL, W. & CAREY, S. 1990. Influence of magma withdrawal on compositional gradients during the AD79 Vesuvius eruption. *Nature,* **345,** 519–521.

SPENCER, K. J. & LINDSLEY, D. H. 1981. A solution model for coexisting iron-titanium oxides. *American Mineralogist,* **68,** 1189–1201.

STORMER, J. C. 1983. The effects of recalculation on estimates of temperature and oxygen fugacity from analyses of multicomponent iron-titanium oxides. *American Mineralogist,* **68,** 586–594.

TOPPING, W. W. & KOHN, B. P. 1973. Rhyolitic tephra marker beds in the Tongariro area, North Island, New Zealand. *New Zealand Journal of Geology and Geophysics,* **16,** 375–395.

VUCETICH, C. G. & PULLAR, W. A. 1973. Holocene tephra formations erupted in the Taupo area and interbedded tephras from other volcanic sources. *New Zealand Journal of Geology and Geophysics,* **16,** 745–780.

WALKER, G. P. L. 1980. The Taupo pumice: product of the most powerful (ultra-plinian) eruption? *Journal of Volcanology and Geothermal Research,* **8,** 69–94.

—— 1981. The Waimihia and Hatepe plinian deposits from the rhyolitic Taupo volcanic centre. *New Zealand Journal of Geology and Geophysics,* **24,** 305–324.

WARE, N. G. 1981. Computer programs and calibration with the PIBS technique for quantitative electronprobe analysis using a lithium-drifted silicon detector. *Computers and Geosciences,* **7,** 167–184.

WILSON, C. J. N. & SMITH, I. E. M. 1985. A basaltic phreatomagmatic eruptive centre at Acacia Bay, Taupo Volcanic Centre. *Journal of the Royal Society of New Zealand,* **15,** 329–337.

—— & WALKER, G. P. L. 1985. The Taupo eruption, New Zealand. I. General aspects. *Philosophical Transactions of the Royal Society of London,* **A314,** 199–228.

——, HOUGHTON, B. F. & LLOYD, E. F. 1986. Volcanic history and evolution of the Maroa-Taupo area, Central North Island. *In:* SMITH, I. E. M. (ed.) *Late Cenozoic Volcanism in New Zealand.* Royal Society of New Zealand Bulletin, **23,** 194–223.

——, ROGAN, A. M., SMITH, I. E. M., NORTHEY, D. J., NAIRN, I. A. & HOUGHTON, B. F. 1984. Caldera volcanoes of the Taupo Volcanic Zone, New Zealand. *Journal of Geophysical Research,* **89,** 8463–8484.

WILSON, L. & WALKER, G. P. L. 1987. Explosive volcanic eruptions VI. Ejecta dispersal in plinian eruptions: the control of eruption conditions and atmospheric properties. *Geophysical Journal of the Royal Astronomical Society,* **89,** 657–679.

Received 7 February 1991; revised typescript accepted 15 October 1991.